Arabian Journal of Chemistry (2022) **15**, 104123

King Saud University

Arabian Journal of Chemistry

www.ksu.edu.sa
www.sciencedirect.com

ORIGINAL ARTICLE

Shellfish waste-derived mesoporous chitosan for impressive removal of arsenic(V) from aqueous solutions: A combined experimental and computational approach

Rachid El Kaim Billah [a], Md. Aminul Islam [b,c,*], Hassane Lgaz [d,*], Eder C. Lima [e], Youness Abdellaoui [f], Youness Rakhila [g], Otman Goudali [a], Hicham Majdoubi [h], Awad A. Alrashdi [i], Mahfoud Agunaou [a], Abdessadik Soufiane [a]

[a] *Department of Chemistry, Faculty of Sciences, Laboratory of Coordination and Analytical Chemistry, University of Chouaib Doukkali, El Jadida, Morocco*
[b] *Department of Arts and Sciences, Faculty of Engineering, Ahsanullah University of Science and Technology (AUST), Tejgaon I/A, Dhaka 1208, Bangladesh*
[c] *Department of Pharmacy and Biomedical Sciences, La Trobe Institute for Molecular Sciences (LIMS), La Trobe University, Bendigo, Australia*
[d] *Innovative Durable Building and Infrastructure Research Center, Center for Creative Convergence Education, Hanyang University ERICA, 55 Hanyangdaehak-ro, Sangrok-gu, Ansan-si, Gyeonggi-do 15588, Republic of Korea*
[e] *Institute of Chemistry, Federal University of Rio Grande do Sul (UFRGS), Porto Alegre, RS, Brazil*
[f] *Faculty of Engineering, Autonomous University of Yucatan, Mérida, Mexico*
[g] *Laboratory of Physical Chemistry and Bioorganic Chemistry, Faculty of Sciences and Technology of Mohammedia, Hassan II University, Mohammedia, Morocco*
[h] *Departments of Chemistry, Faculty of Sciences, Ben M'Sik, Laboratory of Materials and Engineering, University of Hassan II-Casablanca, Morocco*
[i] *Chemistry Department, Umm Al-Qura University, Al-Qunfudah University College, Saudi Arabia*

Received 27 March 2022; accepted 9 July 2022
Available online 16 July 2022

KEYWORDS

Abstract Novel shellfish waste-derived chitosan (CS) has been developed to adsorb As(V) from simulated wastewater under evaluating adsorption process parameters. The coexistence of some

* Corresponding authors.
E-mail addresses: rachidelkaimbillah@gmail.com (R. El Kaim Billah), aminulchem@gmail.com (Md. Aminul Islam), hlgaz@hanyang.ac.kr (H. Lgaz).

Peer review under responsibility of King Saud University.

Production and hosting by Elsevier

https://doi.org/10.1016/j.arabjc.2022.104123

Shrimp shell;
Chitosan;
Arsenic (V);
Adsorption;
Langmuir;
Reusability;
Shellfish;
Molecular dynamic simulation;
Freundlich;
Liu isotherm model

competing ions, like SiO_3^{2-}, Cl^-, NO_3^- and PO_4^{3-} as well as the regeneration capacity of the spent adsorbent, was explored. The experimental data were modeled using several kinetics and isotherm models to understand the mechanism related to the uptake process. As(V) uptake was relatively rapid and highly dependent on pH. The Avrami-fractional-order expression supported data best, while the Liu equation described well isotherm data at pH 5.0. The maximum uptake capability (Liu) was 12.32 mg/g, and the highest removal performance (99 %) was obtained at optimum pH 5.0. Molecular dynamics simulations were performed to more clearly illuminate the atomic-level interactions between arsenic species and CS surface in both acidic and basic mediums. After four adsorption–desorption cycles, CS exhibited more than 90 % As(V) removal efficiency. The results of this study indicates that low cost shellfish derived chitosan is promising for efficient removal of As(V) from water body and can be used to remove other pollutants from watewater.

1. Introduction

Groundwater polluted by arsenic is a serious global concern due to its natural presence, toxicity, and carcinogenicity (Sodhi et al., 2019). Arsenic-contaminated groundwater threatens the well-being of many people worldwide (Biswas et al., 2022). People in South-East-Asian countries like Bangladesh, India, Taiwan, Vietnam, Nepal, and China are severely affected (Das et al., 2021). Arsenic may be introduced to groundwater from a variety of sources, including natural and man-made sources (Varol et al., 2021). Various health complications, including dermatological, skin lesions, cardiovascular, skin cancer, and nervous system, are linked to prolonged intake of arsenic (Palma-Lara et al., 2020). Recently, persistent arsenic (III/V) poisoning has been associated with DNA damage, inhibition of enzyme activities, and tumor promotion (Stevens et al., 2010). Thus, human intake of arsenic is an important issue for concern (Palma-Lara et al., 2020). Despite the adverse effects of arsenic(III/V), more than 200 million people drink arsenic-contaminated water. Both organic and inorganic forms of arsenic are available in the natural environment, and inorganic forms such as As(III) and As(V) are much more prevalent and thus cause further anxiety (Lekit et al., 2013). WHO (World Health Organisation) action level is 10 µg/L, while many countries like Australia, Bangladesh, India, China, and Nepal reported higher than 10 µg/L (Hao et al., 2018).

The treatment of water containing As(V) is a major environmental concern because of its detrimental effects. To reduce the environmental hazards of As(V), As(V)-polluted water must undergo thorough treatment before releasing into the environment. Over a decade, various methods were used for As(V) remediation. These include physicochemical processes such as adsorption using a variety of materials (Abdellaoui et al., 2021, 2020), precipitation, floatation, and coagulation with iron and aluminum compounds (Lakshmanan and Clifford, 2008), ion exchange and membrane separation such as reverse osmosis process (Abejón et al., 2015), oxidation (Nicomel et al., 2015), and biological processes such as phytoremediation (Cimá-Mukul et al., 2019). Among these procedures, precipitation is the most applicable and considered the most economical. However, this method produces enormous amounts of precipitate sludge which require further treatment. Other procedures make it possible to reduce As(V) pollution effectively. However, their application was limited due to several disadvantages, including high operating and maintenance costs, regular inspection of As(V) concentration, membrane fouling and inefficient removal of As(V), including high operating and maintenance costs, regular inspection of the As(V) concentration, clogging of membranes, and ineffective removal of As(V) ions and the need for a pre-treatment stage usually releasing notable amounts of highly toxic sludge and other by-products to be disposed of (Podder and Majumder, 2015). Compared with other procedures, adsorption is considered a cost-effective, safer, and universal method for As(V) decontamination. These advantages have led several research groups to use adsorption to eliminate As(V) from the aquatic environment.

Recently, comprehensive research has been conducted to adsorb As (V) from water. Numerous adsorbents have been used to remove As (V), including iron, aluminum, manganese, zinc, and titanium oxides. (Islam et al., 2018a, 2018b). However, most research is based on oxidative procedures using a wide range of iron minerals and compounds (Hao et al., 2018), such as using magnetite (Liu et al., 2015a), goethite and hematite (Mohapatra et al., 2006), ferrihydrite, and amorphous iron oxide (Huo et al., 2016), mesoporous magnetite nanocomposites (Zubair et al., 2020) and GAC/$MnFe_2O_4$ composites (Podder and Majumder, 2015). In addition, in recent years, metal oxide framework (MOF) materials have achieved very good research results in the treatment of As-containing wastewater (Guan et al., 2020; He et al., 2020a, 2020b; Li et al., 2021; Pandi and Choi, 2021; Zhang et al., 2018, 2021). Other types of adsorbents such as biochar and bone biochar (Alkurdi et al., 2019), MnO and CuO loaded biochar composites (Imran et al., 2021a), TiO_2 (Liu et al., 2015a), carbonaceous nanofiber (Cheng et al., 2016), dried plants (Chiban et al., 2016), palm oil fuel ash (POFA) (Yusof et al., 2020), loam and sandy loam (Rawat et al. 2021), clay mineral (Mohapatra et al., 2007), red mud combined with phosphogypsum (de Souza Costa et al., 2021) and modified saxaul ash (Rahdar et al., 2019), are being increasingly investigated. However, most of these surfaces are less efficient due to their low adsorption capacity and optimal performance at narrow pH ranges. Therefore, many research groups have focused on searching for new classes of adsorbents to adsorb effectively As(V) from contaminated water.

The use of natural polymeric materials such as chitosan for different applications is increasingly considered a simple, inexpensive, efficient, and economical option (Juang et al., 2001; Sharififard et al., 2018; Trung et al., 2006). Chitosan is an important natural polymer, a poly-*N*-glucosamine species formed from the deacetylation of chitin (Pontoni and Fabbricino, 2012). It is strongly hydrophobic and is identified by a chain of flexible polymers and several hydroxyl (–OH) and amino ($–NH_2$) groups with potential adsorption sites. Although chitosan and its derivatives are promising and considered as a low-cost product and easily available, much less recognized and studied is the ability of CS to remove As(V). This performance is associated with the acid-base properties of CS, which led to cationic behavior under acidic situations, more or less significant based on the deacetylation degree of the polymer. Besides, CS is effective in adsorbing metal ions because of the presence of amino and hydroxyl groups that coordinate and electrostatic interaction sites, respectively (Singh et al., 2016b). Recently, chitosan and its derivatives were receiving more and more attention as As(V) removing agents. Chitosan (Mcafee et al., 2001), chitosan thiomer (Singh et al., 2016b), chitosan-modified diatomite (Yadav et al., 2019), functionalized chitosan electrospun (Min et al.,

2016), DMAPAAQ (N, *N*-dimethylamino propyl acrylamide, and methyl chloride quaternary) /FeOOH gel composite (Safi et al., 2019), chitosan and nano chitosan (Kwok et al., 2014), chitosan–red scoria (Ch-Rs) and chitosan–pumice (Ch-Pu) (Girma Asere et al., 2017), chitosan-based porous magnesia loaded alumina (Saha and Sarkar, 2016a), chitosan-coated biosorbent (Boddu et al., 2008), iron-chitosan composite (Gupta et al., 2009), TiO_2 loaded chitosan bead (Miller and Zimmerman, 2010), magnetic nanoparticles loaded chitosan (Wang et al., 2014) and magnetic chitosan nanoparticle (Liu et al., 2015b) were used for As(V) adsorption. However, Moroccan shrimp shell-derived CS has not yet been examined for As(V) uptake and subsequent desorption.

The mechanism of As(V) uptake onto CS-based substrates remains controversial with speculation, including chemisorptions and surface complexation (Kwok et al., 2014). It is reported that transition metal ions uptake onto CS is primarily followed by coordination formation with the unprotonated amino groups, while adsorption of anionic species involves electrostatic attraction with the protonated amino groups (Kwok et al., 2014). As(V) uptake onto metal, oxides have been speculated to involve outer and inner-sphere complexes (mono, bi, and tridentate bond), mono/bidentate corner-sharing complexes, ligand exchange, ion-exchange, and electrostatic interaction (Alkurdi et al., 2019).

In our previous works, we have explored the composition of chitosan-related materials and their composites and also the uptake of Pb(II), Cr(VI), F^-, and Fe(III) from aqueous solutions (Billah et al., 2021a, 2021b, 2021c; El Kaim Billah et al., 2020) This work aims to prepare chitosan (CS) from Moroccan chitin for As(V) adsorption from an aqueous solution in a batch method. The performance of chitosan in As(V) adsorption was studied by evaluating adsorption edges, kinetics, and equilibrium isotherm, the effect of adsorbent dose, the influence of competing anions, and the reusability of the surface. A plausible uptake mechanism has been suggested for understanding the uptake process considering the physic-chemical properties of CS. Furthermore, an FT-IR study was presented before and after As(V) uptake to identify the possible mechanism. Alongside the experimental study, the binding mechanism of As(V) ions on the CS surface was computationally explored by molecular dynamics simulations under solvation conditions. To this end, this report will provide valuable information on large-scale As(V) adsorption where both sustainable and ecological substrates are not readily available, thereby advancing our understanding of As(V) uptake mechanism on naturally available low-cost substrates.

This work mainly deals with the recent application of shellfish waste-derived mesoporous chitosan in As(V) adsorption, particularly emphasizing the As(V) adsorption mechanism. This work is novel in that there is no such study that primarily discusses the As(V) adsorption mechanism.

2. Materials and methods

2.1. Chemicals and adsorbent

Analytical-grade or even better quality chemicals were employed for all purposes and used without further purification. Sodium hydroxide (NaOH, Sigma Aldrich, $\geq$ 99 %), 65 % nitric acid (HNO_3, Sigma Aldrich), 37 % hydrochloric acid (HCl, Sigma-Aldrich) were used as obtained. Sodium hydrogen arsenate heptahydrate ($Na_2HAsO_4{\cdot}7H_2O$, Sigma Aldrich) was employed as an As(V) source. A stock solution of As(V) with a concentration of 1000 mg/L was made in double-distilled water and used as required. Other chemicals used were analytical reagent grades, such as KNO_3, NaCl, NaH2PO$_4$, and Na_2SiO_3. Double distilled water was utilized for all experimental purposes.

The chitosan (poly-B(1–4)-2-amino-2-deoxy-D-glucose) was synthesized from crude chitin extracted from the Moroccan shrimp shells. A schematic representation of the preparation steps of CS is shown in Scheme-I. Firstly, the demineralization was performed using HCl (1 M) (m/v 1:15) at room temperature, and then deproteinization was performed using NaOH (5 %) (m/v 1:20) at 90 °C in flux with gentle stirring for 10 h. Then deacetylation process was followed using NaOH (48 % by weight) at 100C for 6 h with a solid–liquid ratio of 1:20 to remove acetyl groups from chitin. Then the resulting product was washed several times with distilled water until neutral pH was achieved. Finally, the product was dried at 50 °C in an oven and labeled chitosan (CS). The detailed preparation and characterization have been provided elsewhere (Billah et al., 2021a; El Kaim Billah et al., 2020). The XRD analysis confirmed that the as-obtained CS was weakly crystalline, while SEM-EDS showed some holes, cracks, and leaf-shaped morphology and was free from any foreign material. The materials' BET-specific surface area (SBET) was 27.5 m^2/g with a pore diameter of 13.4 nm, implying a mesoporous hierarchical structure. The point of zero charge (pH_{PZC}) obtained by the pH drift method was 6.9. In addition, the FTIR analysis before and after As(V) uptake was performed using a thermo-scientific spectrometer in the region between 400 and 4000 cm^{-1} with a resolution of 4 cm^{-1}. (Scheme 1).

2.2. Adsorption studies

The uptake experiments of As(V) were carried out in duplicate in a batch system in a 50 mL glass reaction vessel by mixing 2 g L^{-1} CS with 50 mL of As(V) solution on a rotary shaker at 600 rpm at 25 °C unless declared otherwise. The initial pH (usually 5.0) of the suspension was maintained by adding HCl (0.1 M) or NaOH (0.1 M) solution dropwise. Kinetic experiments were conducted at various prefixed time intervals, ranging from 10 to 150 min, with an As(V) solution of 16 mg/L at a pH of 5.0. The resulting samples were taken at various fixed time intervals. The influence of pH was investigated by maintaining the pH within 4.0 to 9.0. Reaction vessels were then shaken for 24 h to hydrate the surface functional groups. The impact on As(V) concentration was performed with a concentration of As(V) in the order of 2 to 8 mg/L. The effect of adsorbent dosage was carried out by different amounts of adsorbent in a range of 2–40 g L^{-1} for As (V) adsorption (16 mg/L). The influence of four typical co-existing anions such as phosphate (PO_4^{3-}), silicate (SiO_3^{2-}), chloride (Cl^-), and nitrate (NO_3^-) on As(V) uptake was studied under other optimal experimental conditions. Finally, the regeneration study of the adsorbent after As(V) uptake was conducted using NaOH, NaCl, and HCl as eluent to verify the potential reusability and reliability. In all cases, the residual concentration of As(V) was measured using an Inductive Couple Plasma (ICP) technique.

The amount of As(V) uptake q_e (mg/g) at equilibrium and the percentage of As(V) removal was estimated using the following equations:

$$q_e = \frac{(C_o - C_t)V}{m} \quad \text{(i)}$$

$$\%\,\text{Removal} = \frac{(C_o - C_t)}{C_o} \times 100 \quad \text{(ii)}$$

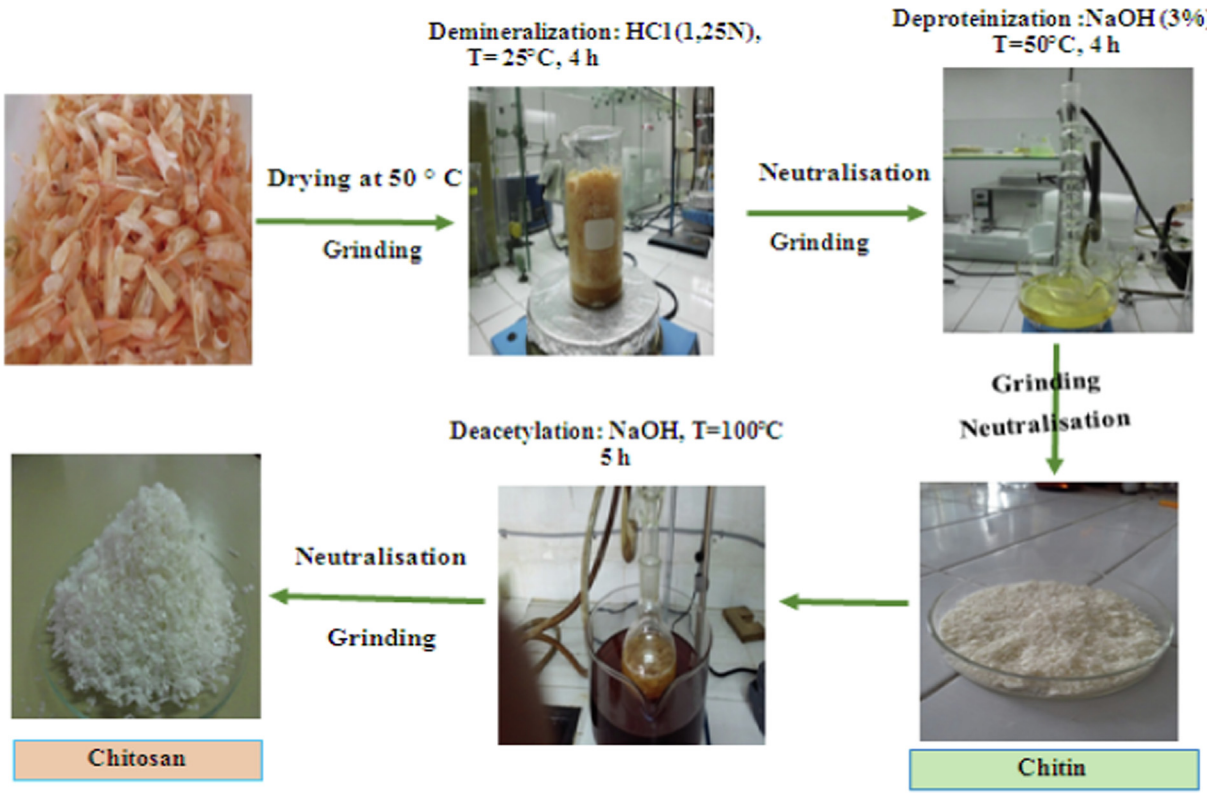

Scheme 1 Schematic demonstration of the preparation steps of chitosan (Cs) from shrimp shells.

Where C_o and C_t express the amounts of initial and adsorbed As (V) in the solution at time t (mg/L), respectively. V represents the solution volume (L), while m denotes the mass of CS (g).

2.3. Uptake data analysis

The knowledge of process kinetics is essential for the practical application of CS for As(V) removal (Lima et al., 2021, 2015). Therefore, As(V) uptake kinetics data were simulated using pseudo-first-order (PFO) and pseudo-second-order (PSO) and Avrami-fractional-order models to understand the chemical nature of the uptake process (Ho and Mckay, 1998; Lagergren, 1898; Weber and Morris, 1963). The models are articulated as follows:

$$q_t = q_1.[1-\exp(-k_1 t)] \quad \text{(iii)}$$

$$q_t = \frac{k_2.q_e^2.t}{1 + q_e.k_2.t} \quad \text{(iv)}$$

$$q_t = q_e.[1 - exp(-k_{AV}.t)^{nAV}] \quad \text{(v)}$$

Where q_e (mg/g) denotes the amount of As(V) adsorbed at equilibrium, q_t (mg/g) represents the amount of As(V) adsorbed at time t. The parameters k_1 (min^{-1}) and k_2 (mg/g min^{-1}), K_{AV} (min^{-1}) are PFO and PSO and Avrami-fractional-order uptake rate constants, respectively.

Besides, the knowledge of equilibrium uptake isotherm allows the identification of the maximum surface coverage and adequately designs the uptake system. Equilibrium isotherm study shows how adsorbate ion distributes between liquid and solid phase in equilibrium.

Therefore, in this study, Langmuir, Freundlich, and Liu models were simulated to explain the obtained equilibrium isotherm data and propose the involved As(V) adsorption mechanism. These equations are articulated as follows (Freundlich, 1906; Langmuir, 1918):

$$q_e = \frac{Q_{max} K_L C_e}{1 + K_L C_e} \quad \text{(vi)}$$

$$q_e = K_F.C_e^{1/nF} \quad \text{(vii)}$$

$$q_e = \frac{Q_{max}.(K_g.C_e)^{nL}}{1 + (K_g.C_e)^{nL}} \quad \text{(viii)}$$

Where q_e is the amount of As(V) adsorbed in mg/g, Q_{max} (mg/g) represents the maximum sorption capacity, K_L (L/mg) and K_g L/mg) represent the Langmuir and Liu equilibrium constant, C_e (mg/L) denotes the concentration of solution at equilibrium. K_F is the Freundlich constant (mg/g) (mg $L^{-1})^{-1/n}$), while n_F and n_L expresses the Freundlich and Liu exponent (dimensionless), respectively.

2.4. Molecular dynamic simulation

Molecular dynamic simulation (MDS) has been performed using the Forcite module implemented in Materials Studio software. Several simulations have been done to investigate the adsorption of arsenate species over the CS surface

(Abdellaoui et al., 2022). To this end, CS crystal structure was cleaved to (0 1 0) direction and extended to (1x1) supercell, comprising two layers. An amorphous cell module was used to create solvent layers that included ten arsenate species without water molecules and in the presence of 50, 200, and 500 water molecules to investigate the effect of solvent on the stability of adsorption. Arsenates adsorption has been simulated using $H_2AsO_4^-$ and $HAsO_4^{2-}$ to investigate the effect of the chemical state on the interaction strength. CS and solvent layers were used to build simulation boxes using the Build module of Materials Studio. Then, all simulation systems were optimized using the Dreiding force field (Mayo et al., 1990). MDS were performed using 2000 ps simulation time, 1 fs time step under NVT ensemble, and Dreiding force field. All other parameters were equivalent to the ''Fine'' quality of the Forcite module.

3. Results and discussion

3.1. Influence of equilibration time

The influence of equilibration time on As(V) uptake on CS is shown in Fig. 1. The adsorption of As (V) by chitosan is relatively fast, with more than 97 % of the arsenic being removed within the first 90 min (Fig. 1), because of the greater abundance of a large number of uptake sites and less resistance to mass transfer at the adsorbent surface, and increases slowly over time until it reaches saturation. This is typical behavior of the uptake process and has been reported previously in other investigations (Abdellaoui et al., 2021). Adsorption achieved equilibrium in approximately 90 min, with an observed removal efficiency of 97.4 %.

3.2. Influence of solution pH

pH is one of the most influential factors in the uptake process (Abou Oualid et al., 2020). The speciation of arsenic is greatly

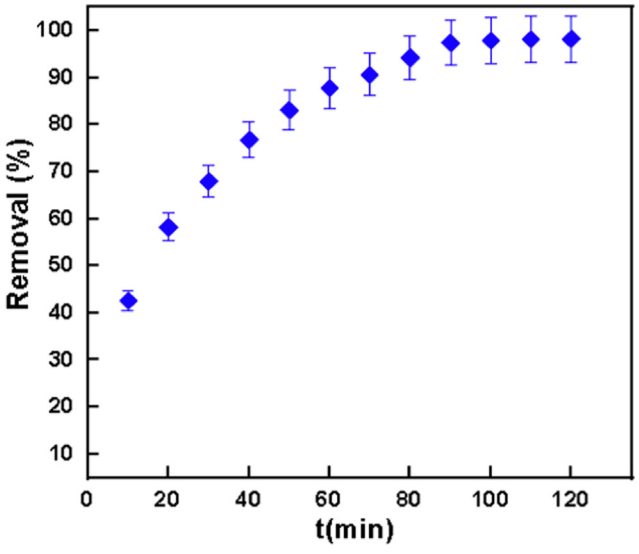

Fig. 1 Impact on equilibration time for As(V) uptake onto Cs. Contact time: 10–150 min; Adsorbent amount = 2.0 g/L; pH = 5.0; $[As(V)]_0$ = 10 mg/L and T = 25 °C.

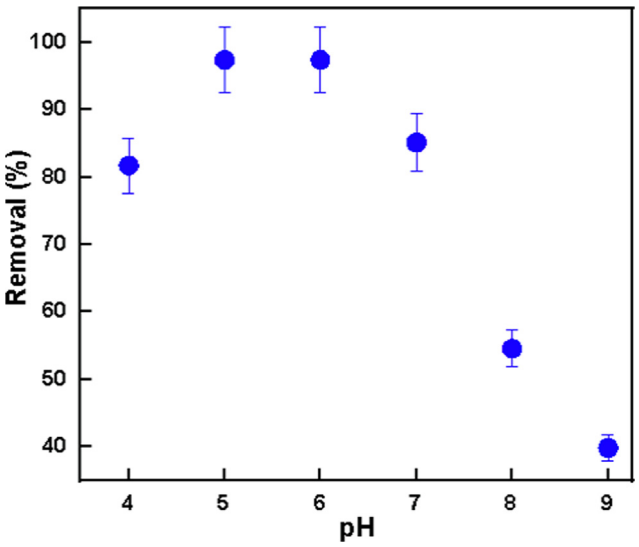

Fig. 2 Impact on solution pH for As(V) uptake onto Cs. Contact time: 90 min; Adsorbent amount = 2.0 g/L; pH = 4.0–9.0; $[As(V)]_0$ = 10 mg/L and T = 25 °C.

dependent on the pH and redox potential of water bodies (Abatal et al., 2018; Singh et al., 2016b). Hence, the pH value of water could notably influence As(V) uptake performance. Therefore, the influence of the initial pH of As(V) solutions on uptake performance of CS was explored for percentage removal of As(V) by varying pH from 4.0 to 9.0. The impact of pH on As(V) uptake onto CS is shown in Fig. 2. It is noted from Fig. 2 that at low pH 4.0, As(V) uptake is lower, and the highest removal of 96 % was achieved at pH 5.0. The percentage removal decreased further with the increase in pH and was nearly 85 % at pH 7.0, 55 % at pH 8.0, and 40 % at pH 9.0. The difference in percentage adsorption as a function of pH could be articulated by the change of the surface charge of CS and the arsenic speciation. As(V) exists mainly as neutral species H_3AsO_4 at pH less than 3. Only the physical adsorption forces between H_3AsO_4 and the substrate were present, leading to lower adsorption. In the range of pH 4.0–6.0, the predominant species is $H_2AsO_4^-$. The amount of $H_2AsO_4^-$ reaches its maximum at pH 5.0, which leads to the strongest electrostatic interaction between $H_2AsO_4^-$ and protonated-amino groups on the surface of the CS; therefore, the optimal pH for the removal of As(V) is 5.0. As(V) is present as a neutral species H_3AsO_4 (pH 1.0–2.5) while it is in the form of anionic species H_2AsO_4 (pH 3–7) and $HAsO_4^{2-}$ (pH 7–12). CS with $-NH_2$ groups are in non-ionic form amongst this range, which results in maximum uptake for ionic As(V) due to strong interaction. Better results of As (V) uptake in acidic pH may be due to the strong electrostatic interaction between protonated CS and anionic H_2AsO_4, which is the predominant species in this pH range. This further confirms the electrostatic nature of the As(V) uptake. Thus, pH 5.0 was chosen as the optimum for As(V) uptake. Similar pH dependence results have been reported for As (V) uptake onto chitosan thiomer (Singh et al., 2016b) and chitosan–red scoria and chitosan–pumice (Ch-Pu) (Girma Asere et al., 2017).

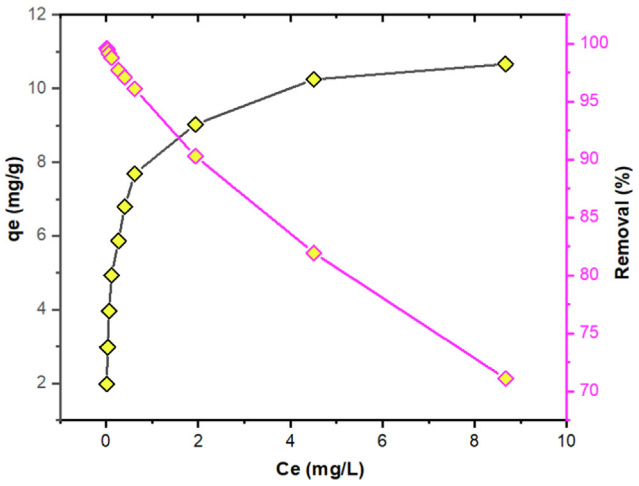

Fig. 3 Effect of initial concentration on As(V) uptake. Contact time: 90 min; Adsorbent amount = 2.0 g/L; $[As(V)]_0$ = 4–30 mg/L, pH = 5.0; and T = 25 °C.

3.3. Influence of initial As(V) concentration

The effect of the initial concentration of As(V) on As(V) uptake was explored by testing various concentrations of adsorbate (4.0–30.0 mg/L). The percentage removal of As (V) is reduced when the initial concentration of As(V) is improved (Fig. 3). The decrease in uptake could be attributed to the higher ratio of As(V) over accessible active substrate sites with increasing As(V) concentration at fixed adsorbent doses. However, the uptake capacity improved with rising initial As(V) concentration until maximum uptake performance (Fig. 3) was achieved at an initial As (V) concentration of 30 mg/L. This is a typically noted phenomenon in the uptake process and has also been observed in other studies for As (V) uptake (Asere et al., 2017; Singh et al., 2016a).

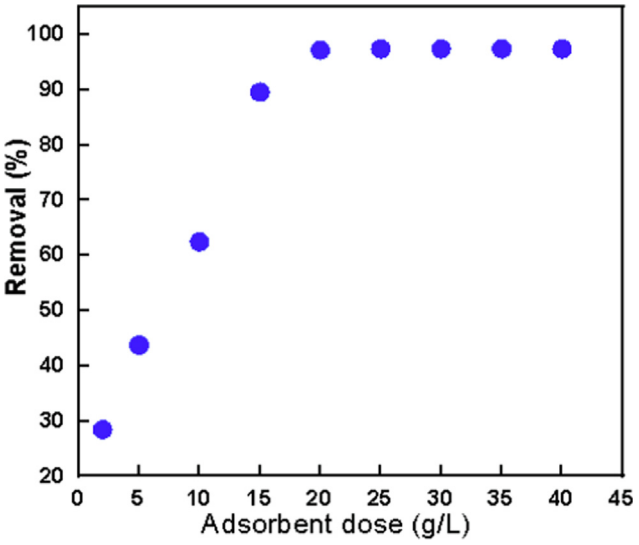

Fig. 4 Effect of adsorbent dosage on As(V) uptake onto Cs. Contact time: 90 min; Adsorbent amount = 0.2–2.0 g/L; pH = 4.0–9.0; $[As(V)]_0$ = 10 mg/L and T = 25 °C.

3.4. Effect of adsorbent dose

The adsorbent amount effect on As(V) uptake was evaluated using different quantities of CS (2–40 g/L) at pH 5.0. The As (V) removal percentage notably increased with rising dose from 2 to 40.0 g/L and thereafter (Fig. 4). The increase in uptake efficiency with an increase in the amount of dose is caused by the larger abundance of active surface sites for As (V) binding at an elevated adsorbent amount (Abdellaoui et al., 2019; Girma Asere et al., 2017). However, above an adsorbent amount of 20.0 g/L, an increase of As(V) removal was negligible, which may be considered the optimal dose. This observation is essential for the actual application of CS for treating As(V) polluted water, especially in developing countries, since CS is a low-cost and locally available adsorbent.

3.5. Adsorption kinetics

The rate expression is an essential factor in understanding the mechanism of As(V) uptake and the performance of the CS for As(V) removal (Saha and Sarkar, 2016a). Adsorption is influenced by the physicochemical process of the surface (Torrik et al., 2019). All time-dependent data were analyzed using PFO, PSO, and Avrami-fractional-order models to understand the nature of uptake. The reliability of the experimental data with the values obtained from the calculation of the model obtained using the adjusted determination coefficients (R^2_{adj}) and the standard deviation of the residues (SD) [56] Fig. 5 and Table 1. The values of R^2_{adj} of Avrami-fractional-order were found to be close to 1.00, and the values of SD were the lowest (Table 1), indicating that the kinetic data were best fitted using this kinetic model. The PFO was the worse model with higher SD values, and PSO was the intermediate kinetic model.

Considering that it is challenging to compare the constant rates of different kinetic models because they present different units, this work employed $t_{1/2}$ and $t_{0.95}$, which present units of time that can be compared. The parameters $t_{1/2}$ and $t_{0.95}$ are

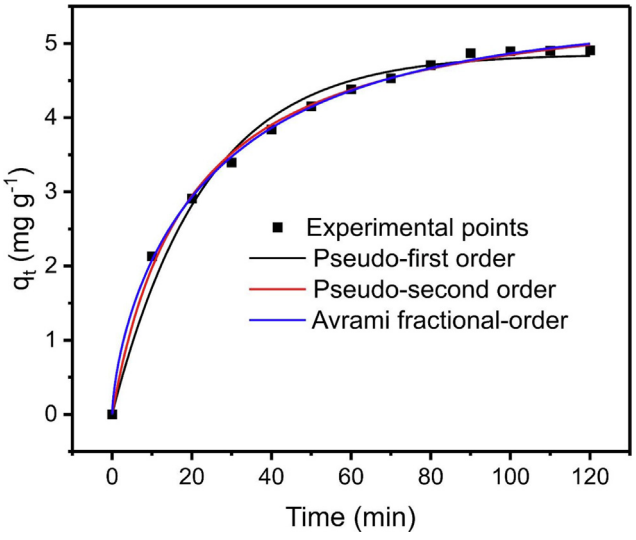

Fig. 5 Pseudo-first-order (*PF1*) (a) and pseudo-second-order (*PS2*) models for As(V) uptake on to CS.

Table 1 Kinetics parameters for As(V) uptake onto CS.

Order	Parameters	Value
Pseudo-first-order (*PS1*)	q_1 (mg/g)	4.861
	k_1 (min^{-1})	0.0433
	$t_{1/2}$ (min)	15.88
	$t_{0.95}$ (min)	66.88
	R^2_{adj}	0.9863
	SD (mg/g)	0.1680
Pseudo-second-order (*PS2*)	q_2 (mg/g)	5.786
	k_2 (g/mg min^{-1})	0.00895
	$t_{1/2}$ (min)	14.61
	$t_{0.95}$ (min)	86.98
	R^2_{adj}	0.9971
	SD (mg/g)	0.07800
Avrami-Fractional-order	q_A (mg/g)	5.345
	k_{AV} (min^{-1})	0.03576
	n_{AV}	0.6909
	$t_{1/2}$ (min)	14.34
	$t_{0.95}$ (min)	87.12
	R^2_{adj}	0.9985

Table 2 Equilibrium isotherm parameters for As(V) uptake onto CS.

Isotherm model	Parameters	Value
Langmuir	Q_{max} (mg/g)	9.953
	K_L (L/mg)	7.799
	R^2_{adj}	0.9537
	SD (mg/g)	0.7409
Freundlich	K_F ((mg/g)(mg/L)$^{-1/nF}$)	7.420
	n_F (dimensionless)	4.860
	R^2_{adj}	0.9587
	SD (mg/g)	0.7000
Liu	Q_{max} (mg/g)	12.32
	K_L (L/mg)	3.631
	nL (dimensionless)	0.5464
	R^2_{adj}	0.9979
	SD (mg/g)	0.1568

the time of attaining 50 % and 95 % saturation, respectively. Furthermore, considering that the Avrami-fractional-order was the best-fitted model, it is necessary to use times of contact between the adsorbent and the adsorbate higher than 90 min to perform the isotherm of adsorption (see Table 1).

3.6. Adsorption isotherm

In order to explore more insight into how As(V) ions were adsorbed over the CS surface, the equilibrium data were fitted using the Langmuir, Freundlich, and Liu isotherms (Fig. 6); the associated parameters are summarized in Table 2. In concordance with the values of R^2_{adj} and SD, the Liu equilibrium model exhibited satisfactory appropriateness for interpreting the adsorption of As(V) ions on the CS adsorbent. Therefore, the suitability of the Liu isotherm model portrayed that the As (V) adsorption process is unique and does not follow ideal monolayer adsorption characteristics.

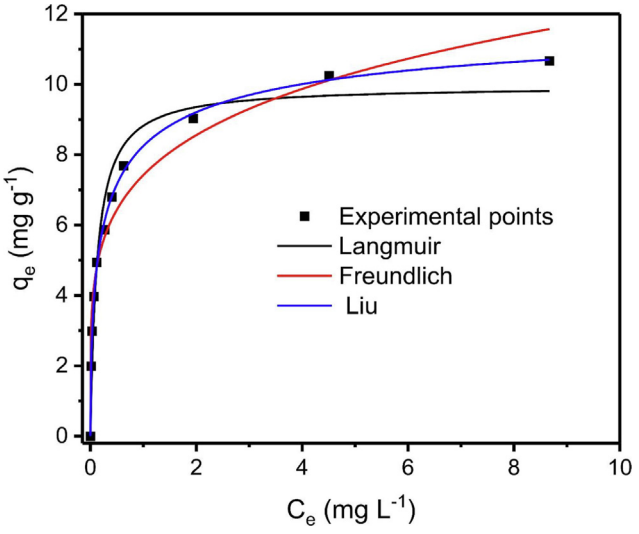

Fig. 6 Non-linear representation of Langmuir isotherm (a) and Freundlich isotherm (b) for As(V) uptake onto Cs.

3.6.1. Comparison of As(V) uptake capacity

In order to justify the applicability of CS as adsorbents for uptake, its uptake capacity must be compared with other various adsorbents used for As(V) uptake. Therefore, the uptake capacity of the CS for As(V) has been further evaluated by comparing the adsorption performance with some other surfaces reported in the literature. However, uptake capacity enormously varies by the surface and experimental conditions, so an accurate comparison of adsorbents is difficult. Table 3 lists the adsorption capacity of different adsorbents. CS has a good adsorption capacity for As(V) among reported surfaces. Besides, the adsorbent has wider pertinence with the pH range. The other substrates listed in Table 3 belong to either uptake performance at a particular pH or are not functional for the speciation.

Moreover, the uptake capacities of some substrates are higher than the levels reported for CS. For example, maximum adsorption capacity for As(V) uptake onto chitosan-based MCS/ZnO@Alg gel microspheres (Wang et al., 2019) and core–shell/bead-like ethylenediamine-functionalized Al-pillared montmorillonite/calcium alginate (Song et al., 2019) were 63.69 mg/g and 61.94 mg/g, respectively. Nevertheless, the data published this at a relatively higher concentration. Therefore, CS has been promising for As(V) uptake from aqueous solutions. The As(V) uptake capacity differences are ascribed to the surface characteristics of each surface structure, functional groups, and specific surface areas (Choong et al., 2007).

3.7. FTIR analysis before and after As(V) adsorption

To explore the notable functional groups responsible for As(V) uptake, Cs was subject to the FTIR study. The FTIR spectra of Cs before and after As(V) uptake is shown in Fig. 7. It is noted from Fig. 7 that the spectrum of Cs exhibits peaks at

Table 3 As(V) adsorption performance with other Cs-based adsorbents.

Adsorbent	pH	Q_{max} (mg/g)	References
Chitosan-modified diatomite	5.0	11.95	(Yadav et al., 2019)
Chitosan thiomer	6.0	17.66	(Singh et al., 2016b)
Chitosan	4.0	58.0	(Kwok et al., 2014)
Chitosan related electrospun nanofiber	7.2	0.5	(Min et al., 2016)
Iron functionalized chitosan-based electrospun nanofiber	7.2	11.2	(Min et al., 2016)
Magnetic chitosan nanoparticle (MCNP)	6.8	65.5	(Liu et al., 2015b)
Chitosan–red scoria (Ch-Rs)	7	0.72	(Girma Asere et al., 2017)
Chitosan-pumice (Ch-Pu)	7	0.71	(Girma Asere et al., 2017)
Chitosan-based porous magnesia impregnated alumina	7.0	17.2	(Saha and Sarkar, 2016a)
Iron-chitosan composite	7	22.5	(Gupta et al., 2009)
TiO_2-impregnated chitosan bead	7.7	2.05	(Miller and Zimmerman, 2010)
Magnetic nanoparticles impregnated chitosan beads	6.8	35.7	(Wang et al., 2014)
Chitosan-based MCS/ZnO@Alg gel microspheres	/	63.69	(Wang et al., 2019)
Core–shell/bead-like ethylenediamine-functionalized Al-pillared montmorillonite/calcium alginate	4.0	61.94	(Song et al., 2019)
Mesoporous chitosan (CS)	5.0	12.32	This study

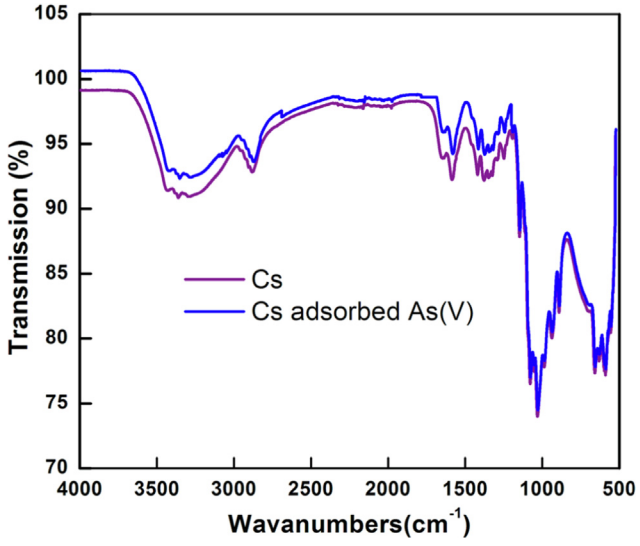

Fig. 7 FT-IR spectra of Cs before and after As(V) uptake onto Cs.

3362 cm^{-1} due to the overlapping of O—H and $–NH_2$ stretching bands, related to extra molecular hydrogen bonding, 2881 cm^{-1} for aliphatic C—H stretching, 1585 cm^{-1} for N—H bending (amide II). 1658 cm^{-1} for deformation of C═O (amide I), it indicates the partially acetylated form of chitin, 1420 and 1375 cm^{-1} for deformation of C—H, 1323 cm^{-1} for C—N (amide II), 1148 cm^{-1}, 1076 $cm^{-1,}$ and 1031 cm^{-1} for C—O—C stretching (an asymmetric stretch of the C—O—C bridge), (skeletal vibration creating the stretch CO) are characteristics of glucosamine residues in chitosan (Saha and Sarkar, 2016b; Singh et al., 2016a).

The peaks originally at 3361.1 cm^{-1}, 2881.5 cm^{-1}, 1658 $cm^{-1,}$ and 1420.2 cm^{-1} were shifted with some decrease in intensity to 3353.4 cm^{-1}, 2876.7 cm^{-1}, 1649.2, and 1416.8 cm^{-1}, there is also a remarkable change in the intensities of the infrared bands after adsorption of As(V) (Singh et al., 2016a). This may be attributed to interference between the functional groups and As (V) during uptake and most likely the existence of H-bonding produced by OH. . ..As, because at acidic pH, the chitosan fractions, initially neutral in Cs, become positively charged, which causes the electrostatic interaction between these groups and the arsenic-negative species of As (V) (Saha and Sarkar, 2016b). Moreover, the well-noted bands centered at about 845 and 1459 cm^{-1} in the spectra after As(V) uptake might be attributed to characteristics vibrations of As-O in $H_2AsO_4^-$ (Saha and Sarkar, 2016b; Singh et al., 2016a). The findings suggest the presence of arsenic species and their binding with Cs via the van der Waals attraction force.

3.8. Effects of competitive anions

It is well-known that multiple cations and anionic species are present in groundwater together with arsenic (Girma Asere et al., 2017). The presence of these ions could influence the As(V) uptake. PO_4^{3-}, SiO_3^{2-}, Cl^- and NO_3^- are generally found in the aquifers, which can compete with arsenic at adsorption sites of adsorbents. Hence, the effect of various common ions (PO_4^{3-}, SiO_3^{2-}, Cl^- and NO_3^-) with different concentrations of 0.1, 0.5, 1, and 10 mM for each ion were chosen to investigate the influence on the uptake capacity of As(V) onto CS (Fig. 8). Before adding these ionic salts, the removal performance of As(V) by CS was 99 %. As shown in Fig. 8, silicate had the largest effect. In contrast, the effect of NO_3^-, PO_4^{3-} and Cl^- is less significant than that of SiO_3^{2-} because they are slightly competing for adsorption sites; indeed, the influence of silicate could be due to a reduction in the surface potential of the CS or a polymerization that can inhibit the adsorption of arsenate by steric effects and can associate with the weak silicic acid species allocation with pH (John et al., 2018). The oxyanion NO_3^-, and PO_4^{3-} did not impact As(V) removal. As a result, the order of competitive ions hindering As(V) uptake was SiO_3^{2-} > Cl^- > NO_3^- > PO_4^{3-}. Similar adverse effects have also been seen in past studies (Girma Asere et al., 2017; Min et al., 2016).

3.9. Thermodynamics of As(V) uptake

Thermodynamic analyses were used to establish a relationship between adsorbent and temperature and to get valuable information to further understand the uptake process (Chiban et al., 2016; Imran et al., 2021b; Rawat et al., 2022). The ther-

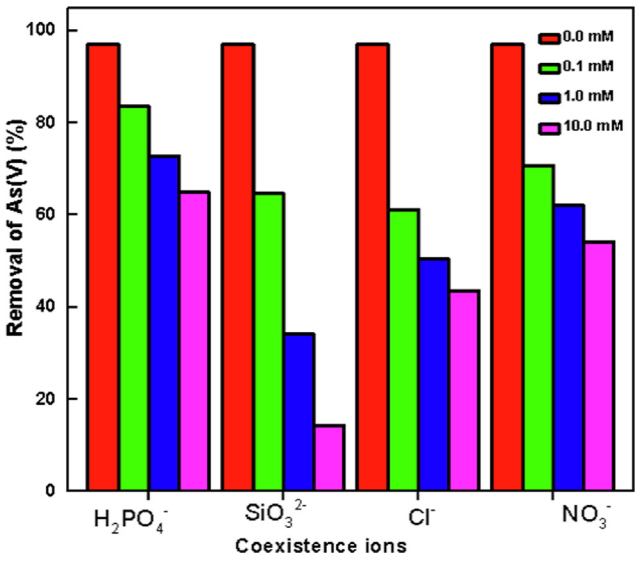

Fig. 8 Effects of coexisting anions on As(V) adsorption onto Cs.

modynamic parameters, namely change of free energy (ΔG), change of enthalpy (ΔH), and change of entropy (ΔS) were determined using equations as follows:

$$Kd = qe/Ce \quad \text{(v)}$$

$$lnKd = \Delta S/R - \Delta H/RT \quad \text{(vi)}$$

$$\Delta G = \Delta H - T\Delta S \quad \text{(vii)}$$

Where q_e (mg g^{-1}) expresses the equilibrium uptake capacity, C_e (mg L^{-1}) denotes solution concentration at equilibrium, K_d denotes uptake equilibrium constant and R represents universal gas constant.

A typical plot of $\ln K_d$ vs 1/T is shown in Fig. 9 for the estimation of thermodynamic parameters. The estimated values of thermodynamic parameters are shown in Table 4. It is noted in Table 4 that the values of ΔG were negative for all studied temperatures implying that As(V) uptake process was spontaneous

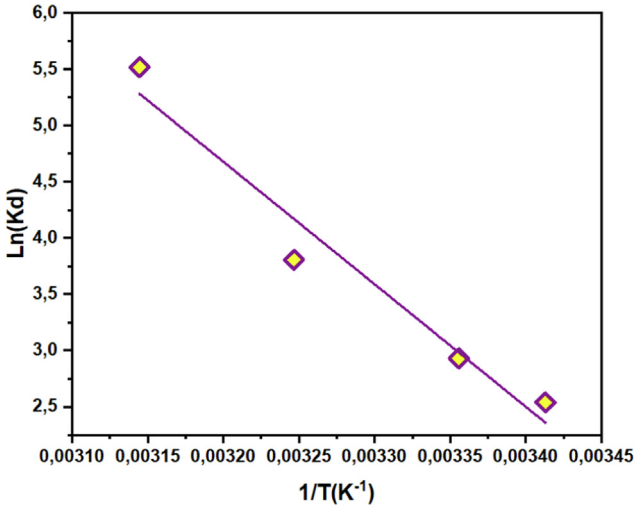

Fig. 9 A plot of ln K_d vs (1/T) for estimation of the thermodynamic parameters for As(V) uptake onto Cs.

(Chiban et al., 2016; Imran et al., 2021b; Rawat et al., 2022). However, the reducing value of ΔG with increasing temperature signifies that the uptake process's spontaneity degree enhances with increasing temperature. The value of change of enthalpy was positive, indicating that the uptake process was endothermic and chemisorption in nature. This finding is also supported by the increase in the value of adsorption capacity with the temperature rise. Moreover, the positive value of entropy indicates that the degrees of free active sites are enhanced at the solid-water interface during the uptake (Liu et al., 2015a). In an aqueous medium, Cs produce hydroxide that can cause structural disorder by ligand exchange with As(V). During uptake, the adsorbed H_2O which is displaced by the surface, As(V) implies some structural changes in the solid-water interface. This provided the existence of randomness in the system (Saha and Sarkar, 2016b).

3.10. Molecular dynamic simulation

Molecular dynamics simulation is a well-recognized computational method that has successfully been used to analyze the adsorption behavior of organic and inorganic species over different adsorbents (Srivastava et al., 2017). In this section, MDS is employed to assess the adsorption of As(V) in its different chemical states over chitosan, aiming to provide additional insights into the adsorption process. To this end, simulations were conducted in a vacuum and different aqueous states for $H_2AsO_4^-$ and $HAsO_4^{2-}$. Ten arsenate species are considered as the reference in all simulations. Fig. 10 **(a, b, c, d)** represents the most stable adsorption configuration of $H_2AsO_4^-$ over the chitosan surface in vacuum, and in the presence of 50, 200, and 500 water molecules, respectively. Inspecting this Figure, we notice that, in the presence of water molecules, some of As(V) species adsorb close to the CS surface while others are directed towards the solvent layer. Most arsenate species tend to adsorb near the CS surface in the vacuum phase. Such behavior can be explained by the competitive adsorption between arsenate species and water molecules for the CS surface. However, visual inspection is far from accurate in describing adsorbate adsorption strength over the CS surface. Therefore, results can be more accurately described by estimating the energy of interaction between adsorbates and adsorbent's surface. The interaction energy of arsenic species over CS surface in vacuum phase is −44.65 kcal/mol. Adding 50 water molecules into the simulation box increases the interactive forces, leading to an −82.03 kcal/mol interaction energy. For simulation boxes including a higher number of water molecules, interaction energies are −129.07 and −139.36 kcal/mol, respectively, for 200 and 500 water molecules. It can be observed that the solvent has a positive effect on the adsorption strength of arsenate species. In other words, this notable difference between interaction energies in vacuum and aqueous phase signifies that adsorbate species do not strongly interact with solvent molecules. Furthermore, the fact that the interaction energy becomes more significant with a higher amount of water signifies that the solvent has a stabilization effect (Abdellaoui et al., 2021).

To extend the discussion of the above results, simulations are performed in a basic medium under the same conditions. Arsenate species are simulated here using $HAsO_4^{2-}$, which characterizes a basic medium, as shown in the above-mentioned

Table 4 Thermodynamic parameters for As(V) uptake onto Cs.

Adsorbent	ΔH° (KJ/mol)	ΔS° (J/mol. K)	ΔG° (KJ/mol)			
			298 K	303 K	313 K	323 K
Cs	91.37	328.85	−6.18	−7.26	−9.74	−14.59

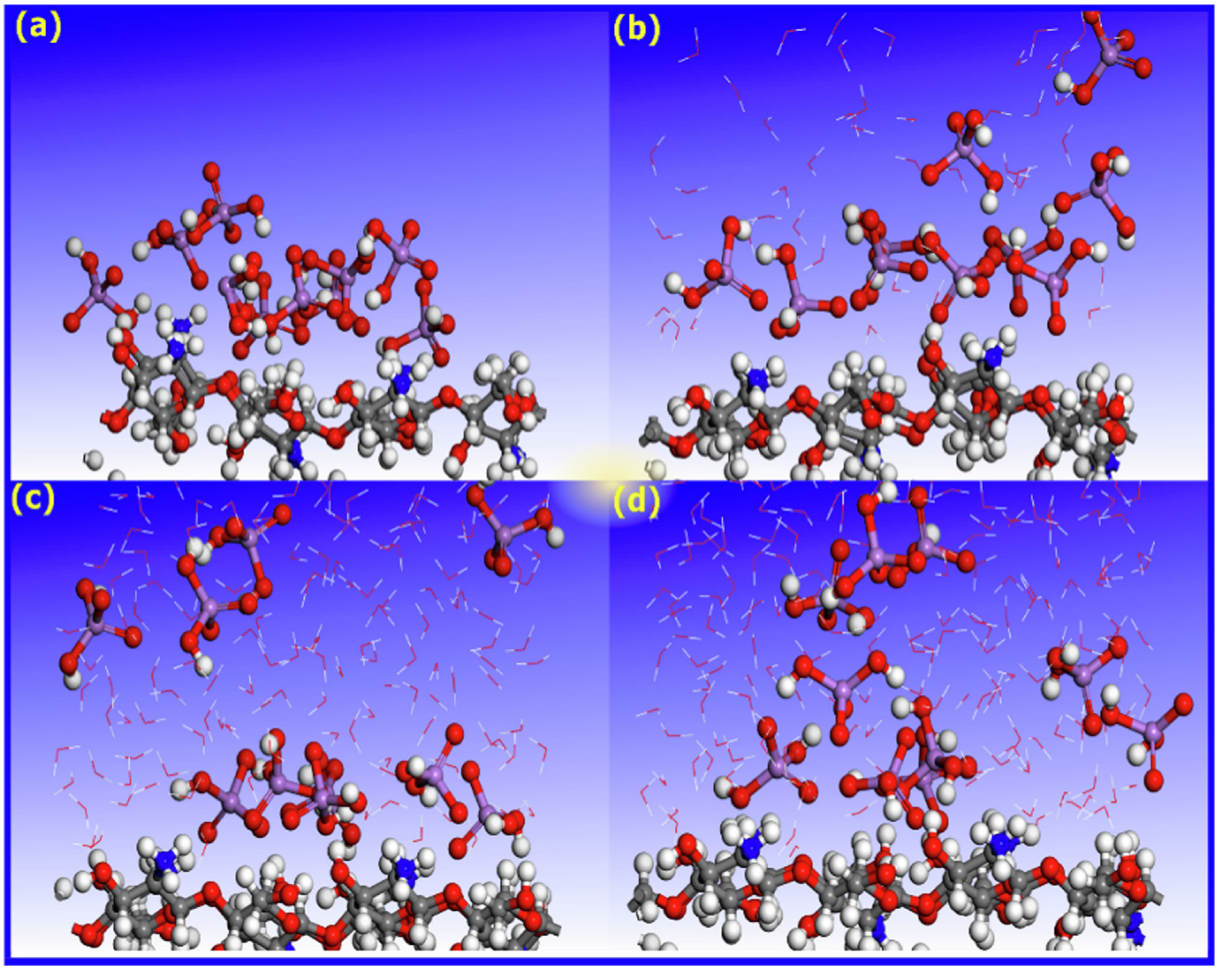

Fig. 10 The most stable adsorption configurations of $H_2AsO_4^-$ arsenate species on Cs(0 1 0) surface are obtained by molecular dynamics simulation; (a) Vacuum state, (b)-(d) in presence of 50, 200, and 500 water molecules, respectively.

results. The most stable adsorption configurations are shown in the supplementary material (**Fig. S1**). However, energetic outcomes are the most important in investigating the effect of the basic medium on the interactive forces of arsenate species compared to the acidic medium.

Results show a substantial decrease in interaction energy values for all systems. For example, it shows interaction energies of −35.46 kcal/mol in a vacuum and −70.53, −70.04, −69.33 kcal/mol in the presence of 50, 200, and 500 water molecules, respectively. Besides, it can be noted that the solvent has a strong negative effect on the adsorption strength of arsenate species, leading to a decreased interaction energy value with an increase in water amount. This behavior suggests that arsenate species probably have strong interactions with solvent molecules, negatively affecting their adsorption over the CS surface. Similar results were recently reported on the adsorption of arsenate species over fly ash-based zeolites (Abdellaoui et al., 2021). Together, these results confirm the experimental ones that demonstrated a low adsorption capacity of arsenates in the basic medium.

3.11. Elucidation of As(V) adsorption mechanisms

Based on experimental data with the exploration of isotherms, kinetics model, and FTIR analysis and surface functional groups, the stepwise mechanisms of As(V) uptake onto CS can be as follows:

(i) Electrostatic interaction between the positively charged center (OH) and negatively charged As(V) species and under acidic conditions (pH < pH_{PZC} = 6.9) (Hao et al., 2018).
(ii) The negatively charged arsenic species ($AsO_3$3- or H_2AsO3- and $AsO_4$3- or $H_2AsO_4^-$) bind via electrostatic attraction to CS functional groups (Hao et al., 2018). The FTIR findings established this character of attractive force between CS and As(V) because of the formation of a new peak at near 845 cm-1, the feature of O—H...As vibration band on the arsenic laden CS (Saha and Sarkar, 2016b). With an increase in solution pH, the surface gradually achieved negative charges, which repelled As(V), and therefore As(V) adsorbed by the electrostatic attraction in basic solution was prevented (Saha and Sarkar, 2016b).
(iii) The formation of surface complexation, including both outer and inner sphere, might be a notable pathway for the elimination of As(V) (Hao et al., 2018)
(iv) The ligand or ion-exchange reactions between positively charges surface center and $AsO_3$3- or H_2AsO_3- and $AsO_4$3- or H_2AsO_4- (Hao et al., 2018; Podder and Majumder, 2015). This was also established by forming a broad peak at 3420 cm-1 in the FTIR study (Saha and Sarkar, 2016b).
(v) Surface precipitation or condensation of metal hydroxides onto CS may also occur (Hao et al., 2018) and
(vi) The mesoporous spaces of CS can be filled by the As(V) during uptake (physisorption) (Hao et al., 2018).

The proposed stepwise mechanisms for As(V) adsorption onto CS are shown in Fig. 11.

3.12. Regeneration and reusability of spent adsorbent

Substrate regeneration is a notable aspect to be evaluated in an uptake process (Girma Asere et al., 2017). In this study, the capacities of CS to regenerate after adsorption of As(V) using three desorbing agents such as NaOH, NaCl, and HCl, with a concentration of 0.5 M were used as eluent. According to the results, 0.5 M NaOH exhibited the best desorption efficiency along with all solvents (Fig. 12a). The regeneration of CS was studied in 6 adsorption–desorption cycles (Fig. 12**b**), and the removal efficiency was still 99.7 % after three cycles. However, after five cycles, the performance decreased by 24 %, i.e., the porous structure attributed to CS. The result suggested that the prepared CS could decontaminate As(V) ions at least 6 times. The data implies that the CS showed satisfactory reusability, and the CS can be used to treat As(V) polluted water. Similar findings were reported for regenerating magnetic chitosan nanoparticles (Liu et al., 2015b) and chitosan-modified materials (Girma Asere et al., 2017).

4. Conclusion

The adsorption of As(V) by chitosan (CS) was performed with a variation of equilibration time, pH, mass, and initial As(V) concentration and was considered a cheap and environmentally friendly, and naturally available bio-adsorbent. The extent of As(V) adsorption was rapid and notably influenced by a combination of factors, including experimental parameters and the coexistence of substances. Kinetic study showed that the As(V) uptake was fast in the first 90 min and thereafter increased slowly to sufficient equilibrium in approximately 2 h. The maximum As(V) removal was achieved at pH, and this pH value, 97.4 % As(V), was removed. The *PS2* model is the most suitable to describe the uptake kinetics of arsenic, and the established adsorp-

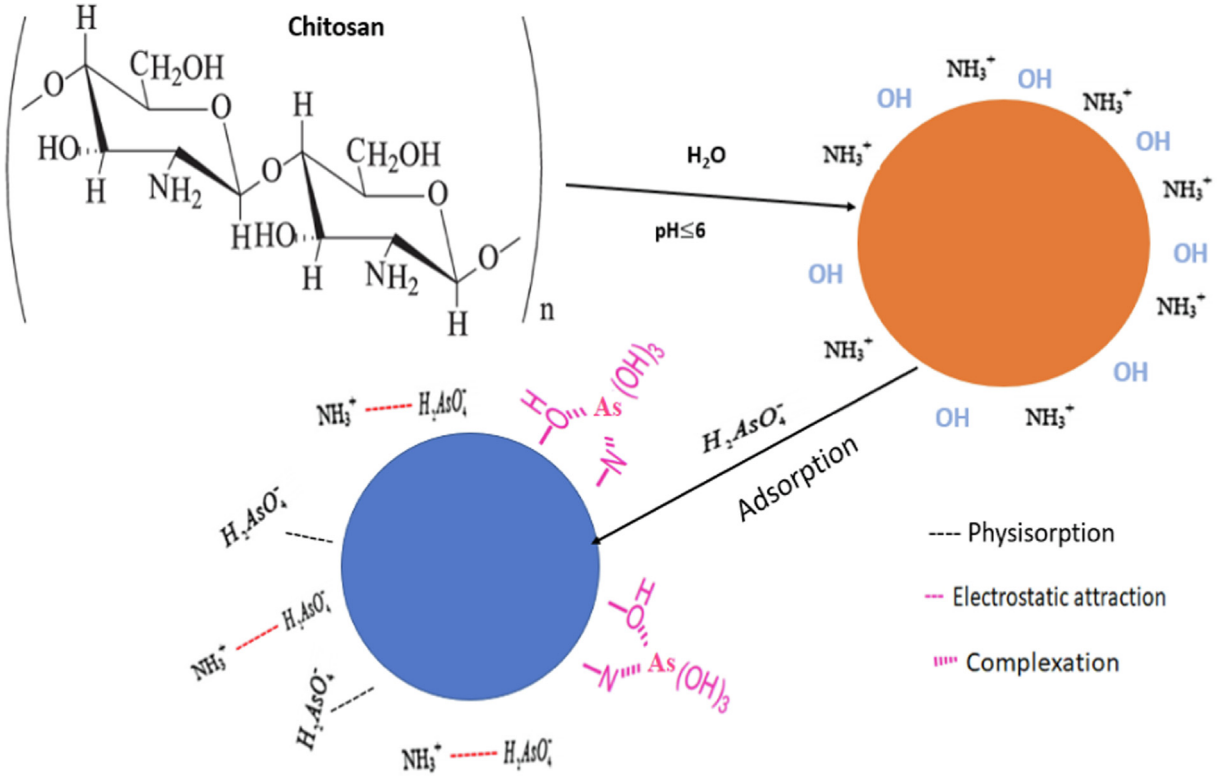

Fig. 11 Proposed As(V) uptake mechanism onto CS.

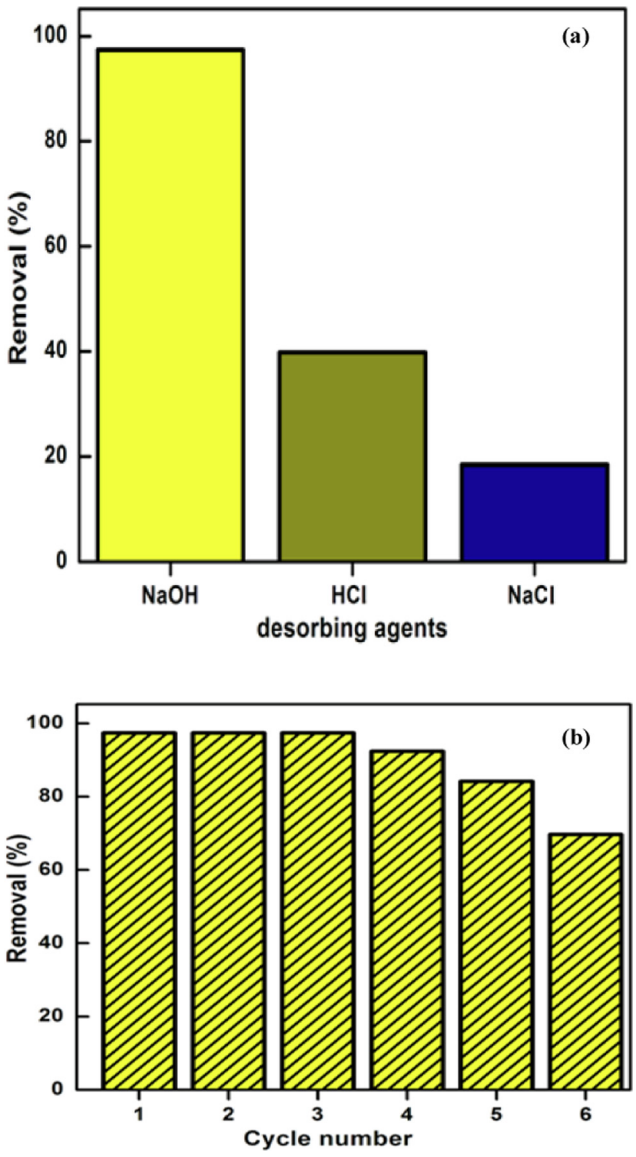

Fig. 12 (a) Percentages (%) of As(V) recovered by different eluting agents and (b) Adsorption-desorption cycles for As(V) recovered by CS.

tion isotherms showed that the adsorption of arsenic by CS is perfectly correlated with the Langmuir model. The maximum monolayer performance capacity was 8.19 mg/g. Finally, the regeneration test shows the possibility of recycling the CS for wastewater treatment containing As (V) ions at least 6 times without a notable reduction in adsorption capacity. Based on the macroscopic findings and surface properties of CS, the interaction mechanism between CS and As(V) was proposed to be physisorption, van der Waals attraction, ion-exchange, surface complexation, and electrostatic attraction for charged species. The SiO_3^{2-} co-ion had a strong competitive influence on As(V) uptake efficiency, while PO_4^{3-}, Cl^- and NO_3 ions had little influence on As(V) removal. Molecular dynamics simulations were carried out to shed light on the As(V) ions adsorption mechanism under basic and acid conditions on the CS surface. The energetic outcomes showed a strong negative effect on the adsorption strength of arsenate species in the basic medium.

Most importantly, the removal performance of As(V) showed no notable decrease after six adsorption–desorption cycles. The result of this study shows that a negligible amount of CS is sufficient to adsorb a notable concentration of As(V), and the substrate can be employed for adsorption of various pollutants from large-scale environmental samples from both industrial wastewater (sparingly acidic) and natural groundwater (pH 7.0). The primary advantageous uptake findings produced for As(V) will advance further research on the practical applicability of the cheaply synthesized adsorbent.

Declaration of Competing Interest

The authors declare that they have no known competing financial interests or personal relationships that could have appeared to influence the work reported in this paper.

Acknowledgments

This research was done as a part of the Ph.D. project pollutants removal using low-cost adsorbents supported by the Department of Chemistry, University of Chouaib Doukkali. The authors would like to thank the Deanship of Scientific Research at Umm Al-Qura University for supporting this work by Grant Code: (22UQU4331100DSR01).

Appendix A. Supplementary data

Supplementary data to this article can be found online at https://doi.org/10.1016/j.arabjc.2022.104123.

References

Abatal, M., Olguin, M.T., Abdellaoui, Y., El Bouari, A., 2018. Sorption of Cd(II), Ni(II) and Zn(II) on natural, sodium-, and acid-modified clinoptilolite-rich tuff. Environ. Prot. Eng. 44, 42–59. https://doi.org/10.5277/epe180104.

Abdellaoui, Y., Olguin, M.T., Abatal, M., Bassam, A., Giácoman-Vallejo, G., 2019. Relationship between Si/Al ratio and the sorption of Cd(II) by natural and modified clinoptilolite-rich tuff with sulfuric acid. Desalin. Water Treat. 150, 157–165. https://doi.org/10.5004/dwt.2019.23792.

Abdellaoui, Y., Gamero-Melo, P., Díaz-Jiménez, L., Ponce-Caballero, C., Giácoman-Vallejos, G., 2020. Synthesis and Surface Modification of Small Pore Size Zeolite W for Improving Removal Efficiency of Anionic Contaminants from Water. Bull. Environ. Contamin. Toxicol. 105, 934–940. https://doi.org/10.1007/s00128-020-03036-z.

Abdellaoui, Y., El Ibrahimi, B., Abou Oualid, H., Kassab, Z., Quintal-Franco, C., Giácoman-Vallejos, G., Gemero-Melo, P., 2021. Iron-zirconium microwave-assisted modification of small-pore zeolite W and its alginate composites for enhanced aqueous removal of As(V) ions: Experimental and theoretical studies. Chem. Eng. J. 421,. https://doi.org/10.1016/j.cej.2021.129909 129909.

Abdellaoui, Y., Celaya, C.A., Elhoudi, M., Boualou, R., Agalit, H., Reina, M., Gamero-Melo, P., Oualid, H.A., 2022. Understanding of vibrational and thermal behavior of bio-based doped alginate@nickel cross-linked beads: A combined experimental and theoretical study. J. Mol. Struct. 1249,. https://doi.org/10.1016/j.molstruc.2021.131524 131524.

Abejón, A., Garea, A., Irabien, A., 2015. Arsenic removal from drinking water by reverse osmosis: Minimization of costs and energy consumption. Sep. Purif. Technol. 144, 46–53. https://doi.org/10.1016/j.seppur.2015.02.017.

Abou Oualid, H., Abdellaoui, Y., Laabd, M., Ouardi, M.E., Brahmi, Y., Iazza, M., Oualid, J.A., 2020. Eco-Efficient Green Seaweed Codium decorticatum Biosorbent for Textile Dyes : Characterization, Mechanism, Recyclability, and RSM Optimization. ACS Omega. https://doi.org/10.1021/acsomega.0c02311.

Alkurdi, S.S.A., Herath, I., Bundschuh, J., Al-Juboori, R.A., Vithanage, M., Mohan, D., 2019. Biochar versus bone char for a sustainable inorganic arsenic mitigation in water: What needs to be done in future research? Environ. Int. https://doi.org/10.1016/j.envint.2019.03.012.

Asere, T.G., Verbeken, K., Tessema, D.A., Fufa, F., Stevens, C.V., Du Laing, G., 2017. Adsorption of As(III) versus As(V) from aqueous solutions by cerium-loaded volcanic rocks. Environ Sci Pollut Res 24, 20446–20458. https://doi.org/10.1007/s11356-017-9692-z.

Billah, R.E., Kaim, Y.H., Otman Goudali, M.A., Abdessadik, S., 2021a. Removal and Regeneration of Iron (III) from Water Using New Treated Fluorapatite Extracted from Natural Phosphate as Adsorbent. Biointerface Res. Appl. Chem 11, 13130–13140.

Billah, R.E.K., Khan, M.A., Park, Y.K., Am, A., Majdoubi, H., Haddaji, Y., Jeon, B.H., 2021b. A comparative study on hexavalent chromium adsorption onto chitosan and chitosan-based composites. Polymers 13, 1–15. https://doi.org/10.3390/polym13193427.

Billah, R.E.K., Khan, M.A., Wabaidur, S.M., Jeon, B.H., Amira, A. M., Majdoubi, H., Haddaji, Y., Agunaou, M., Soufiane, A., 2021c. Chitosan/phosphate rock-derived natural polymeric composite to sequester divalent copper ions from water. Nanomaterials 11, 1–17. https://doi.org/10.3390/nano11082028.

Biswas, S., Sahoo, S., Debsarkar, A., 2022. Social Vulnerability of Arsenic Contaminated Groundwater in the Context of Ganga-Brahmaputra-Meghna Basin: A Critical Review. In: Geospatial Technology for Environmental Hazards. Springer Nature, pp. 39–61. https://doi.org/10.1007/978-3-030-75197-5_3.

Boddu, V.M., Abburi, K., Talbott, J.L., Smith, E.D., Haasch, R., 2008. Removal of arsenic (III) and arsenic (V) from aqueous medium using chitosan-coated biosorbent. Water Res. 42, 633–642. https://doi.org/10.1016/j.watres.2007.08.014.

Cheng, W., Ding, C., Wang, X., Wu, Z., Sun, Y., Yu, S., Hayat, T., Wang, X., 2016. Competitive sorption of As (V) and Cr (VI) on carbonaceous nanofibers 293, 311–318. https://doi.org/10.1016/j.cej.2016.02.073.

Chiban, M., Carja, G., Lehutu, G., Sinan, F., 2016. Equilibrium and thermodynamic studies for the removal of As(V) ions from aqueous solution using dried plants as adsorbents. Arabian J. Chem. 9, S988–S999. https://doi.org/10.1016/j.arabjc.2011.10.002.

Choong, T.S.Y., Chuah, T.G., Robiah, Y., Gregory Koay, F.L., Azni, I., 2007. Arsenic toxicity, health hazards and removal techniques from water: an overview. Desalination 217, 139–166. https://doi.org/10.1016/j.desal.2007.01.015.

Cimá-Mukul, C.A., Abdellaoui, Y., Abatal, M., Vargas, J., Santiago, A.A., Barrón-Zambrano, J.A., 2019. Eco-Efficient Biosorbent Based on Leucaena leucocephala Residues for the Simultaneous Removal of Pb(II) and Cd(II) Ions from Water System: Sorption and Mechanism. Bioinorg. Chem. Appl. 2019, 1–13. https://doi.org/10.1155/2019/2814047.

Das, A., Joardar, M., De, A., Mridha, D., Chowdhury, N.R., Khan, B.K., M.T., Chakrabartty, P., Roychowdhury, T.,, 2021. Pollution index and health risk assessment of arsenic through different groundwater sources and its load on soil-paddy-rice system in a part of Murshidabad district of West Bengal. India. Groundwater for Sustainable Development 15,. https://doi.org/10.1016/j.gsd.2021.100652 100652.

de Souza Costa, E.T., Guilherme, L.R.G., Lopes, G., de Lima, J.M., Curi, N., 2021. Sorption of cadmium, lead, rasenate, and phosphate on red umd combined with phosphogypsum. Int. J. Environ. Res. 15, 427–444.

El Kaim Billah, R., Abdellaoui, Y., Anfar, Z., Giácoman-Vallejos, G., Agunaou, M., Soufiane, A., 2020. Synthesis and Characterization of Chitosan/Fluorapatite Composites for the Removal of Cr (VI) from Aqueous Solutions and Optimized Parameters. Water Air Soil Pollut. 163, 1–14. https://doi.org/10.1007/s11270-020-04535-9.

Freundlich, H.M.F., 1906. Over the Adsorption in Solution. The Journal of Physical Chemistry 57, 385–471.

Girma Asere, T., Mincke, S., De Clercq, J., Verbeken, K., Tessema, D. A., Fufa, F., Stevens, C.V., Laing, G.Du, Naidu, R., Rahman, M. M., Wijayawardena, A., 2017. Removal of Arsenic (V) from Aqueous Solutions Using Chitosan-Red Scoria and Chitosan-Pumice Blends. Int. J. Environ. Res. Public Health. https://doi.org/10.3390/ijerph14080895.

Guan, T., Li, X., Fang, W., Wu, D., 2020. Efficient removal of phosphate from acidified urine using UiO-66 metal-organic frameworks with varying functional groups. Appl. Surf. Sci. 501, 144074.

Gupta, A., Chauhan, V.S., Sankararamakrishnan, N., 2009. Preparation and evaluation of iron–chitosan composites for removal of As (III) and As (V) from arsenic contaminated real life groundwater. Water Res. 43, 3862–3870.

Hao, L., Liu, M., Wang, N., Li, G., 2018. A critical review on arsenic removal from water using iron-based adsorbents. RSC Adv. https://doi.org/10.1039/c8ra08512a.

He, J., Xu, Y., Shao, P., Yang, L., Sun, Y., Yang, Y., Cui, F., Wang, W., 2020a. Modulation of coordinative unsaturation degree and valence state for cerium-based adsorbent to boost phosphate adsorption. Chem. Eng. J. 394, 124912.

He, J., Xu, Y., Wang, W., Hu, B., Wang, Z., Yang, X., Wang, Y., Yang, L., 2020b. Ce (III) nanocomposites by partial thermal decomposition of Ce-MOF for effective phosphate adsorption in a wide pH range. Chem. Eng. J. 379, 122431.

Ho, Y.S., Mckay, G., 1998. KINETIC MODELS FOR THE SORPTION OF DYE FROM AQUEOUS SOLUTION BY WOOD. Trans IChemE 76, 183–191.

Huo, L., Zeng, X., Su, S., Bai, L., Wang, Y., 2016. Enhanced removal of As (V) from aqueous solution using modified hydrous ferric oxide nanoparticles Institute of Environment and Sustainable Development in Agriculture OPEN. Sci. Rep. 7, 1–12. https://doi.org/10.1038/srep40765.

Imran, M., Iqbal, M.M., Iqbal, J., Shah, N.S., Khan, Z.U.H., Murtaza, B., Amjad, M., Ali, S., Rizwan, M., 2021. Synthesis, characterization and application of novel MnO and CuO impregnated biochar composites to sequester arsenic (As) from water: Modeling, thermodynamics and reusability. J. Hazard. Mater. 401,. https://doi.org/10.1016/j.jhazmat.2020.123338 123338.

Islam, M.A., Morton, D.W., Johnson, B.B., Pramanik, B.K., Mainali, B., Angove, M.J., 2018a. Metal ion and contaminant sorption onto aluminium oxide-based materials: A review and future research. J. Environ. Chem. Eng. 6, 6853–6869.

Islam, M.A., Morton, D.W., Johnson, B.B., Mainali, B., Angove, M. J., 2018b. Manganese oxides and their application to metal ion and contaminant removal from wastewater. J. Water Process Eng. 26, 264–280. https://doi.org/10.1016/j.jwpe.2018.10.018.

John, Y., David, V.E., Mmereki, D., 2018. A Comparative Study on Removal of Hazardous Anions from Water by Adsorption: A Review. Int. J. Chem. Eng. 2018, 1–21.

Juang, R.-S., Wu, F.-C., Tseng, R.-L., 2001. Solute adsorption and enzyme immobilization on chitosan beads prepared from shrimp shell wastes. Bioresour. Technol. 80, 187–193. https://doi.org/10.1016/S0960-8524(01)00090-6.

Kwok, K.C.M., Koong, L.F., Chen, G., McKay, G., 2014. Mechanism of arsenic removal using chitosan and nanochitosan. J. Colloid Interface Sci. 416, 1–10. https://doi.org/10.1016/j.jcis.2013.10.031.

Lagergren, s.,, 1898. Zur Theorie Der Sogenannten Adsorption Geloster Stoffe. Kungliga Svenska Vetenskapsakademiens.

Lakshmanan, D., Clifford, D.A., 2008. Arsenic removal by coagulation With aluminum, iron, titanium, and zirconium. J- American Water Works Assoc. 100, 76–88.

Langmuir, I., 1918. the Adsorption of Gases on Plane Surfaces of Glass, Mica and Platinum. J. Am. Chem. Soc. 40, 1361–1403. https://doi.org/10.1021/ja02242a004.

Lekit, B.M., Markovit, D.D., Rajakovit-Ognjanovit, V.N., Yukit, A. R., Rajakovit, L.V., 2013. Arsenic Removal from Water Using Industrial By-Products. J. Chem. 2013. https://doi.org/10.1155/2013/121024.

Li, S., Zhang, Q., Yin, C., Chen, J., Yang, X., Wang, S., 2021. Tuning microscopic structure of Al-based metal-organic frameworks by changing organic linkers for efficient phosphorus removal. J. Cleaner Prod. 292, 125998.

Lima, É.C., Adebayo, M.A., Machado, F.M., 2015. Kinetic and Equilibrium Models of Adsorption. In: Bergmann, C.P., Machado, F.M. (Eds.), Carbon Nanomaterials as Adsorbents for Environmental and Biological Applications. Springer International Publishing, Cham, pp. 33–69. https://doi.org/10.1007/978-3-319-18875-1_3.

Lima, E.C., Sher, F., Guleria, A., Saeb, M.R., Anastopoulos, I., Tran, H.N., Hosseini-Bandegharaei, A., 2021. Is one performing the treatment data of adsorption kinetics correctly? J. Environ. Chem. Eng. 9,. https://doi.org/10.1016/j.jece.2020.104813 104813.

Liu, C.-H., Chuang, Y.-H., Chen, T.-Y., Tian, Y., Li, H., Wang, M.-K., Zhang, W., 2015a. Mechanism of Arsenic Adsorption on Magnetite Nanoparticles from Water: Thermodynamic and Spectroscopic Studies. Environ. Sci. Technol. 49, 7726–7734. https://doi.org/10.1021/acs.est.5b00381.

Liu, C., Wang, B., Deng, Y., Cui, B., Wang, J., Chen, W., He, S.-Y., 2015b. Performance of a new magnetic chitosan nanoparticle to remove arsenic and its separation from water. J. Nanomater. 2015, 1–9. https://doi.org/10.1155/2015/191829.

Mayo, S.L., Olafson, B.D., Goddard, W.A., 1990. DREIDING: A generic force field for molecular simulations. J. Phys. Chem. 94, 8897–8909. https://doi.org/10.1021/j100389a010.

Mcafee, B.J., Gould, W.D., Nadeau, J.C., da Costa, A.C.A., 2001. Biosorption of metal ions using chitosan, chitin and biomass of rhizopus oryzae. Sep. Sci. Technol. 36, 3207–3222. https://doi.org/10.1081/SS-100107768.

Miller, S.M., Zimmerman, J.B., 2010. Novel, bio-based, photoactive arsenic sorbent: TiO2-impregnated chitosan bead. Water Res. 44, 5722–5729.

Min, L.-L., Zhong, L.-B., Zheng, Y.-M., Liu, Q., Yuan, Z.-H., Yang, L.-M., 2016. Functionalized chitosan electrospun nanofiber for effective removal of trace arsenate from water. Sci. Rep. 6, 32480. https://doi.org/10.1038/srep32480.

Mohapatra, D., Mishra, D., Chaudhury, G.R., Das, R.P., 2007. Arsenic adsorption mechanism on clay minerals and its dependence on temperature. Korean J. Chem. Eng. 24, 426–430. https://doi.org/10.1007/s11814-007-0073-z.

Mohapatra, M., Sahoo, S.K., Anand, S., Das, R.P., 2006. Removal of As(V) by Cu(II)-, Ni(II)-, or Co(II)-doped goethite samples. J. Colloid Interface Sci. 298, 6–12. https://doi.org/10.1016/j.jcis.2005.11.052.

Nicomel, N.R., Leus, K., Folens, K., Van Der Voort, P., Du Laing, G., 2015. Technologies for Arsenic Removal from Water: Current Status and Future Perspectives ijerph13010062–ijerph13010062 Int. J. Environ. Res. Public Health 13. https://doi.org/10.3390/ijerph13010062.

Palma-Lara, I., Martínez-Castillo, M., Quintana-Pérez, J.C., Arellano-Mendoza, M.G., Tamay-Cach, F., Valenzuela-Limón, O.L., García-Montalvo, E.A., Hernández-Zavala, A., 2020. Arsenic exposure: A public health problem leading to several cancers. Regul. Toxicol. Pharm. 110,. https://doi.org/10.1016/j.yrtph.2019.104539 104539.

Pandi, K., Choi, J., 2021. Selective removal of anionic ions from aqueous environment using iron-based metal-organic frameworks and their mechanistic investigations. J. Mol. Liq. 329, 115367.

Podder, M.S., Majumder, C.B., 2015. Removal of arsenic by a Bacillus arsenicus biofilm supported on GAC/MnFe2O4 composite. Groundw. Sustain. Dev. 1, 105–128. https://doi.org/10.1016/j.gsd.2015.11.002.

Pontoni, L., Fabbricino, M., 2012. Use of chitosan and chitosan-derivatives to remove arsenic from aqueous solutions - A mini review. In: Carbohydrate Research. Elsevier, pp. 86–92. 10.1016/j.carres.2012.03.042.

Rahdar, S., Taghavi, M., Khaksefidi, · Razieh, Ahmadi, S.,, 2019. Adsorption of arsenic (V) from aqueous solution using modified saxaul ash: isotherm and thermodynamic study. Appl. Water Sci. 9, 87. https://doi.org/10.1007/s13201-019-0974-0.

Rawat, A.P., Kumar, V., Pratibha Singh, A.C.S., 2021. Kinetic behavior and mechanism of arsenate adsorption by loam and sandy loam soil. Soil Sed. Contam.: A Int. J.

Rawat, A.P., Kumar, V., Singh, P., Shukla, A.C., Singh, D.P., 2022. Kinetic behavior and mechanism of arsenate adsorption by loam and sandy loam soil. Soil Sed. Contam.: A Int. J. 31, 15–39.

Safi, S.R., Senmoto, K., Gotoh, T., Iizawa, T., Nakai, S., 2019. The effect of γ-FeOOH on enhancing arsenic adsorption from groundwater with DMAPAAQ + FeOOH gel composite. Sci. Rep. 9, 11909. https://doi.org/10.1038/s41598-019-48233-x.

Saha, S., Sarkar, P., 2016a. Arsenic mitigation by chitosan-based porous magnesia-impregnated alumina: performance evaluation in continuous packed bed column. Int. J. Environ. Sci. Technol. 13, 243–256. https://doi.org/10.1007/s13762-015-0806-1.

Saha, S., Sarkar, P., 2016b. Differential pulse anodic stripping voltammetry for detection of As (III) by Chitosan-Fe (OH) 3 modified glassy carbon electrode: A new approach towards speciation of arsenic. Talanta 158, 235–245.

Sharififard, H., shahraki, Z.H., Rezvanpanah, E., Rad, S.H.,, 2018. A novel natural chitosan/activated carbon/iron bio-nanocomposite: Sonochemical synthesis, characterization, and application for cadmium removal in batch and continuous adsorption process. Bioresour. Technol. 270, 562–569. https://doi.org/10.1016/j.biortech.2018.09.094.

Singh, P., Chauhan, K., Priya, V., Singhal, R.K., 2016b. A greener approach for impressive removal of As(iii)/As(v) from an ultra-low concentration using a highly efficient chitosan thiomer as a new adsorbent. RSC Adv. 6, 64946–64961. https://doi.org/10.1039/C6RA10595E.

Singh, D.K., Mohan, S., Kumar, V., Hasan, S.H., 2016a. Kinetic, isotherm and thermodynamic studies of adsorption behaviour of CNT/CuO nanocomposite for the removal of As (III) and As (V) from water. RSC Adv. 6, 1218–1230.

Sodhi, K.K., Kumar, M., Agrawal, P.K., Singh, D.K., 2019. Perspectives on arsenic toxicity, carcinogenicity and its systemic remediation strategies. Environ. Technol. Innovation 16,. https://doi.org/10.1016/j.eti.2019.100462 100462.

Song, Y., Wang, S., Yang, L.-Y., Yu, D., Wang, Y.-G., Ouyang, X., 2019. Facile fabrication of core–shell/bead-like ethylenediamine-functionalized Al-pillared montmorillonite/calcium alginate for As (V) ion adsorption. Int. J. Biol. Macromol. 131, 971–979.

Srivastava, R., Kommu, A., Sinha, N., Singh, J.K., 2017. Removal of arsenic ions using hexagonal boron nitride and graphene nanosheets: A molecular dynamics study. Mol. Simul. 43, 985–996. https://doi.org/10.1080/08927022.2017.1321754.

Stevens, J.J., Graham, B., Walker, A.M., Tchounwou, P.B., Rogers, C., 2010. The effects of arsenic trioxide on DNA synthesis and genotoxicity in human colon cancer cells. Int. J. Environ. Res. Public Health 7, 2018–2032. https://doi.org/10.3390/ijerph7052018.

Torrik, E., Soleimani, M., Ravanchi, M.T., 2019. Application of kinetic models for heavy metal adsorption in the insgle and multicomponent adsorption system. Int. J. Environ. Res. 13, 813–828. https://doi.org/10.1007/s41742-019-00219-3.

Trung, T.S., Thein-Han, W.W., Qui, N.T., Ng, C.-H., Stevens, W.F., 2006. Functional characteristics of shrimp chitosan and its membranes as affected by the degree of deacetylation. Bioresour. Technol. 97, 659–663. https://doi.org/10.1016/j.biortech.2005.03.023.

Varol, M., Gündüz, K., Sünbül, M.R., 2021. Pollution status, potential sources and health risk assessment of arsenic and trace metals in agricultural soils: A case study in Malatya province. Turkey. Environmental Research 202. https://doi.org/10.1016/j.envres.2021.111806.

Wang, S., Lu, Y., Ouyang, X., Liang, X.X., Yu, D., Yang, L.-Y., Huang, F., 2019. Fabrication of chitosan-based MCS/ZnO@ Alg gel microspheres for efficient adsorption of As (V). Int. J. Biol. Macromol. 139, 886–895.

Wang, J., Xu, W., Chen, L., Huang, X., Liu, J., 2014. Preparation and evaluation of magnetic nanoparticles impregnated chitosan beads for arsenic removal from water. Chem. Eng. J. 251, 25–34.

Weber, W.J., Morris, J.C., 1963. Kinetics of Adsorption on Carbon from Solutions. Journal of the Sanitary Engineering Division 89, 31–60.

Yadav, M., Goswami, P., Paritosh, K., Kumar, M., Pareek, N., Vivekanand, V., 2019. Seafood waste: a source for preparation of commercially employable chitin/chitosan materials. Bioresour. Bioprocess. 6, 1–20. https://doi.org/10.1186/s40643-019-0243-y.

Yusof, M.S.M., Othman, M.H.D., Wahab, R.A., Jumbri, K., Razak, F.I.A., Kurniawan, T.A., Abu Samah, R., Mustafa, A., Rahman, M.A., Jaafar, J., Ismail, A.F., 2020. Arsenic adsorption mechanism on palm oil fuel ash (POFA) powder suspension. J. Hazard. Mater. 383,. https://doi.org/10.1016/j.jhazmat.2019.121214 121214.

Zhang, Z., Chen, Z., Xiao, Y., Yi, M., Zheng, X., Xie, M., Shen, M., 2021. Study of the dynamic adsorption and the effect of the presence of different cations and anions on the adsorption of As (V) on GUT-3. Appl. Organomet. Chem. 35, e6289.

Zhang, C., Xiao, Y., Qin, Y., Sun, Q., Zhang, S., 2018. A novel highly efficient adsorbent ${$[Co4 (L) 2 (μ3-OH) 2 (H2O) 3 (4, 4′-bipy) 2]·(H2O) 2$}$ n: synthesis, crystal structure, magnetic and arsenic (V) absorption capacity. J. Solid State Chem. 261, 22–30.

Zubair, Y.O., Fuchida, S., Tokoro, C., 2020. Insight into the mechanism of arsenic(III/V) uptake on mesoporous zerovalent iron-magnetite nanocomposites: adsorption and microscopic studies. ACS Appl. Mater. Interf. 12, 49755–49767. https://doi.org/10.1021/acsami.0c14088.